Partial Leaching Effect to Pt decorated Pd-Fe/C Nanoparticles for Oxygen Reduction Reaction

Libo Zhang[1], Xiaoran Wang[1], Maryam Bayati[2], Ben Bin Xu[2], Terence Xiaoteng Liu[2,*], Hong Zhu[1*]

[1]State Key Laboratory of Chemical Resource Engineering, Institute of Modern Catalysis, Department of Organic Chemistry, college of chemistry, Beijing University of Chemical Technology, North Third Ring Road 15, Chaoyang District, Beijing, 100029, China

E-mail: zhuho128@126.com;

[2]Department of Mechanical and Construction Engineering, Faculty of Engineering and Environment, Northumbria University, Newcastle upon Tyne, NE1 8ST, UK

E-mail: terence.liu@northumbria.ac.uk

Summary

A facile route to produce high performance Pt@Pd-Fe/C oxygen reduction reaction (ORR) catalysts are explained in this article. The surface modification of partial leaching of Fe from Pd-Fe nanoparticles (NPs) followed by Pt decoration using microwave-assisted method has largely enhanced the catalytic performances. Herein, we show that alloying Pd with Fe atoms improves the catalytic activity toward ORR by expending lattices to tune the strain and ligand effect. Further modification by partially leaching Fe atoms from the core surface can increase the active sites, the trace amounts of Pt decorated on the modified Pd-Fe cores improved the ORR activity and stability by controlling the strain effect and ligand effect between Pt, Fe and Pd. Such a special designed structure interacts to give further improved the ORR catalytic performances which is higher than commercial Johnson Matthey (JM) Pt/C catalysts, and shed a light of mass production low-cost catalyst.

KEYWORDS：

Oxygen reduction reaction; low Pt content; partial leaching; modification; durability

1.Introduction

Among all renewable energy systems, proton exchange membrane fuel cell (PEMFC) has been considered as the most important renewable energy source for electric vehicles (EVs), due to excellent fuel efficiency, low-operating temperature, high power density, and low maintenance cost.[1–5] However, major technical issues which limit the mass production of PEMFCs are the scarcity of high loading of Pt nano-catalyst and limited performance especially for oxygen reduction reaction (ORR).[6–9] Therefore, usage of non-precious metal catalysts would be of great benefit in accelerating commercialization of PEMFCs. Numerous efforts have been made to develop high performances, low platinum or non Pt catalysts for ORR especially by employing Pt-like element with similar and enhanced properties.[10–18]

Pd and Pt have both FCC crystal structure and with very close lattice constant. Investigations showed that Pd based catalysts, Pd-M catalyst (M=Co, Fe, Cu, Ni or Cr), outperform Pt for the ORR. This is due to the synergistic impact between Pd and those transition metals, which enhances its ORR activity.[19–21] However, the Pd based catalyst show the poor durability under the harsh condition, which limited the practical application.[22-23] One of the strategies of improving the stability of Pd nanoparticles is to alloy with transition metal to form PdM nanoparticles with novel structures, this will increase the stability over single Pd element catalyst. A thin layer of Pt as decoration could further improve the stability as it will form protection layers and keep Pd from dissolving during electrochemical reaction.[24-27] Liu and his coworkers synthesized Pd@Pt/C core-shell structured alloy catalyst using the polyol method. The Pd core and Pt shell interact to each other, which enhances the activity and stability through strain effect and ligand effect between Pt and Pd.[28] Wang *et al.* showed that the surface strain of Pd nanocatalyst is tuned with adding Fe and Co which improved its oxygen reduction activity.[29] It is shown that a thin layer of Pt improves the stability and simultaneously the activity of the Pd catalyst through the strain and ligand effects between the two metals. Luo *et al.* synthesized Pt@Cu catalysts by chemical dealloying,[30] the Pt-Cu alloy was prepared by microwave-assisted method, then added HNO_3 solution to the reaction system to remove Cu atoms to synthesize core-shell structure Pt@Cu catalysts.

In this study, we prepared Pd-Fe nanoparticles and used weak HNO_3 acid to partially

leached Fe atoms to increase the surface Pd atoms. After decoration with ultralow amount of Pt, the catalyst showed comparable ORR catalytic activity to JM commercial catalyst (code) with high durability and low cost. This is a new approach for mass production of ORR catalyst, and it could accelerate the commercialization of PEMFC and it powered automobiles.

2.Experimental

The modified Pt@Pd-Fe/C catalysts (denoted as M-Pt@Pd-Fe/C, M stands for 'modified') were synthesized using a two-step reduction method. The carbon-supported Pd-Fe/C alloy catalyst was prepared followed by weak acid treatment to partially remove Fe to obtain M-Pd-Fe/C. The removal of the surface Fe atoms resulted in an increase in active surface sites which facilitate the Pt decoration. This is the step that M-Pd-Fe/C nanoparticles have been prepared as the core. Then the core was decorated by Pt atoms on the surface denoted as M-Pt@Pd-Fe/C. Catalyst structure characterizations and catalytical properties were analysed using various spectroscopic, microscopic and electrochemical methods. The M-Pt@Pd-Fe/C catalysts demonstrated high catalytic performance for ORR. Scheme 1 shows the complete synthesis process of M-Pt@Pd-Fe/C.

2.1 Reagents and Materials

All reagents are of analytical grade. Ferric nitrate ($Fe(NO_3)_3\,9H_2O$), hexachloroplatinic acid ($H_2PtCl_6\,6H_2O$), palladium chloride ($PdCl_2$), nitric acid (HNO_3), perchloric acid ($HClO_4$), ethylene glycol (EG), potassium hydroxide (KOH) and sodium borohydride ($NaBH_4$) were obtained from J&K. Carbon black (Vulcan XC-72R) was bought from Beijing Reagent Co. Ltd (China) and oxidized by hydrogen peroxide. Commercial Pt/C catalysts (denoted as JM Pt/C, 40 wt%, HISPEC4000) were obtained from Johnson Matthey. Nitrogen of 99.99% was purchased from Beijing Industrial Gas Co. Ltd. and used to keep an inert atmosphere for drying process.

2.2. Catalysts Preparation

M-Pt@Pd-Fe/C and Pt@Pd-Fe/C catalysts are synthesized through a two-step synthesis

process. First, carbon powder (Vulcan XC-72R), as support materials, was pretreated by hydrogen peroxide to form oxygenous functional groups and removed any impurities. Then 49.851mg of $Fe(NO_3)_3\ 9H_2O$, 6.03ml of $PdCl_2$ solution (24g/L) and 80mg treated carbon powder were mixed with 40 mL ethylene glycol (EG) under a stirring condition at room temperature for about 0.5 hours. Then the pH of the solution was changed to 9 by 10 wt% KOH/EG solution. $NaBH_4$ solution (1M, 8mL) was added to the suspension, followed by further stirring for 4 hours. The content was centrifuged, rinsed by deionized water and alcohol for three times. The paste was initially dried at 80 ºC in an oven overnight, and heated at 200 ºC under N_2 (99.99%) atmosphere for 2 hours. The obtained sample was denoted as Pd-Fe/C. For comparison, the Pd/C catalysts were obtained using the same synthesis procedure.

To increase the surface Pd atoms, the Pd-Fe/C is leached in acid to remove any excess Fe on the surface of the sample. The obtained catalyst powder was dispersed in deionized water using ultrasonic sound bath and 0.1M HNO_3 acid solution was added slowly to remove Fe atoms while stirring for 2hours. The suspension was centrifuged, rinsed by deionized water and alcohol for three times, filtered and dried at 80ºC overnight. The obtained sample was denoted as M-Pd-Fe/C.

To decorate M-Pd-Fe/C with Pt atoms, 60mg of the M-Pd-Fe/C powder was added in 30 mL of EG solution and mixed with 0.426mL of $H_2PtCl_6\ 6H_2O$ solution (3g/L) to make Pd: Pt nominal atomic ratio of 30:1. The pH of the mixture was changed to 9 by using 10 wt% KOH in EG. The composite was stirred at room temperature for about one more hour, followed by heating in a microwave reactor at 80ºC for 30 min to completely reduce the platinum precursor. The obtained sample (M-Pt@Pd-Fe/C) were separated, cleaned and dried at 80 ºC in an oven for analysis. The Pt@Pd-Fe/C catalysts were prepared by a similar procedure on untreated Pd-Fe/C catalyst for comparison.

2.3. Physical characterization

The X-ray powder diffraction (XRD, Shimadzu XD-3A diffractometer, Japan) was used to record the crystal phase of the catalysts. Transmission electron microscope (TEM, JEOL3010HR) was used to understand the morphology and particles size distribution. The

plasma atomic emission spectroscopy system (ICP-AES, USA, Agilent Technologies) and energy-dispersive X-ray (EDX) was used to record the catalysts' actual composition. The elemental distribution and physical structure was studied by the scanning transmission electron microscopy-high angle annular dark field (STEM-HAADF) with energy dispersive spectrometer (EDS) (JEOL JEM ARM200F); the electronic property of Pt element was investigated by an X-ray photoelectrons spectrometer (XPS, LAB250ESCA).

2.4 Electrochemical test

The electrochemical test was conducted using a Germany Zahner electrochemical workstation. The cyclic voltammetry (CV) and linear sweep voltammetry (LSV) were tested using a three-electrode cell under room temperature (25 ± 2 ºC), consisting of a working electrode, the reference electrode (Ag/AgCl electrode), and the counter electrode (Pt wire). A glassy carbon (GC) rotating disk electrode (RDE, Tianjin Aida, 5 mm in diameter) served as the working electrode. Potentials are reported versus reversible hydrogen electrode (RHE). The catalysts ink (1mg/ml) was obtained by ultrasonically mixing the catalysts, 25 wt% isopropanol in deionized water and 5 wt% Nafion solution. The working electrodes were prepared by covering the thin layer of catalysts ink on the polished GC electrodes with catalyst loading (and metal loading). The CV test was conducted in $HClO_4$ electrolyte (0.1 M, N_2 saturated). During the test, the scan range is between 0.025 and 1.075 V vs. RHE, and the scan rate was 50 mV s^{-1}. Moreover, the LSV tests were conducted in an O_2 saturated 0.1 M $HClO_4$ electrolyte at 1600 rpm in a scan range between 0.05 and 1.1 V vs. RHE with scan rate of 10 mV s^{-1}.

3. Results and discussion

3.1 Structural and compositional results

The Fig.1 shows the XRD results of all obtained catalysts. The broad peak at around 2θ=25º is attributed to the (200) crystal phase from the carbon support. The peaks at 2θ=39.7, 45.4, and 67.1º correspond to the (111), (200), and (220) planes of Pd metal (PDFcard # 46-1043) and Pt metal (PDFcard # 04-0802), respectively.[31] The (111) peak of Pd-Fe/C at 2θ=41.2º attributes to the alloy phase of Pd-Fe, a positive shift can be observed over this

peak of Pd/C, this is the evidence of Fe atom alloyed into the lattice of the Pd. Pd has larger atomic radius than Fe, which results in an increase in crystallinity reflected an increase of peak intensity.[32–34] The peaks of M-Pd-Fe/C have a negative shift in comparison with Pd-Fe/C, This could be caused by partial removal of Fe element from the surface. No separated Fe peaks were observed in the XRD spectrum of Pd-Fe/C and M-Pd-Fe/C catalysts, indicating that Fe is presented in an alloy form. Peak position of Pt@Pd-Fe/C and M-Pt@Pd-Fe/C slightly shifted to lower angles when the modified cores are decorated with Pt atoms, which is caused by the increase in lattice parameter of Pt atoms, because Pt has larger atomic radius than Fe and Pd.[35] This is the evidence of existence of Pt atoms which later in this paper is confirmed by other techniques.[30]

The morphology of M-Pd-Fe/C and M-Pt@Pd-Fe/C catalysts and their histograms of particle size distribution are displayed in Fig.2. As shown in Fig. 2(a) and 2(b), the TEM images indicate that the metal nanoparticles are uniformly distributed without obvious agglomeration. The M-Pd-Fe/C and M-Pt@Pd-Fe/C catalysts show narrow particle size distribution. The average particle sizes are calculated to be 4.14 and 4.85 nm, respectively. The increase in particle size proves M-Pd-Fe cores are decorated by platinum atoms.[36] The high resolution transmission electron microscopy (HRTEM) images of the catalysts display the lattice fringes and the distance between d-spacings of 0.2252nm and 0.2260nm for M-Pd-Fe/C (Fig.2(c)) and M-Pt@Pd-Fe/C (Fig.2(d)), respectively. The Pd-Fe particles are more favorable for Pt deposition in compare to the carbon support, because the Pt atoms have the same crystal phase structure as Pd, and large amount of active sites which serve as the seed for Pt to grow.[37] The Pd-Fe/C and Pt@Pd-Fe/C catalysts are also included in **Fig.S1,** TEM images show similar structural characteristics.

For examining the elemental distribution and microstructure of M-Pt@Pd-Fe/C NPs, we conducted HAADF/STEM in association with EDS elemental mapping. Fig.3 (a)-(f) shows the HAADF/STEM images of M-Pt@Pd-Fe/C catalyst and the corresponding elemental mapping images (EDS). The Pd and Fe atoms are highly alloyed. The EDS elemental mapping show Pt atoms deposited on the surface of M-Pd-Fe/C particle.

The metal contents of the catalysts measured by EDX and ICP are supplied in Table 1. ICP-AES result indicates the content of Pd, Fe and Pt is consistent with the nominal

composition and the existence of Fe atoms in Pd-Fe/C even after acid leaching were not reduced during the experiments compared to actual atomic ratio of Fe and Pd. Fig.4 demonstrates the XPS Pt 4f region spectrum of Pt@Pd-Fe/C, M-Pt@Pd-Fe/C, and JM Pt/C catalysts. the three peaks at about 71.0, 72.4, and 74.8eV, which can be attributed to the Pt $4f_{7/2}$ peaks of Pt_0, Pt_{II}, and Pt_{IV}, respectively, demonstrating that the Pt on the surface have three oxidation states.[30] As observed from the spectrum, Pt 4f binding energy peak position of the Pt@Pd-Fe/C, M-Pt@Pd-Fe/C showed negative shifted comparing to JM Pt/C, demonstrating that Fe and Pd elements can modify the electronic properties of Pt. And the binding energy of M-Pt@Pd-Fe/C catalyst shows further negative shifted energy position compared to Pt@Pd-Fe/C catalysts. The negative shift demonstrates a downshift of d-band centre of M-Pt@Pd-Fe/C catalysts, which reduce the binding strength of the adsorbed intermediates.[38] From the above results, the M-Pt@Pd-Fe/C catalysts were successfully prepared and the lower binding energy is beneficial to promote the ORR.

3.2 Electrochemical tests

The electrochemical CV test was conducted in N_2-saturated $HClO_4$ electrolyte (0.1 M), the curves' potential has been converted in respect to RHE. Fig.5 (a) shows CV curves of JM Pt/C, M-Pd-Fe/C, Pt@Pd-Fe/C, and M-Pt@Pd-Fe/C. The peaks of the oxygen reduction is around 0.75V vs. RHE and the peak of the hydrogen oxidation peak is near to 0.05V vs. RHE.[39] Electrochemical surface area (ECSA) was calculated according to the integrated charge of the hydrogen absorption area in the potential range between 0.05 and 0.4V with 2.1 C/m^2 as a conversion factor. Pd also could influence the ECSA in our catalysts, so the ECSA of the obtained catalysts was estimated according to the following equation:[40]

$$ECSA_{\text{noble metal}}\ (m^2/g) = Q_H/(2.1*[\text{noble metal}]) \quad (1)$$

Where 'noble metal' represents the mass of Pt and Pd, Q_H is the total electric quantity of the hydrogen desorption. The calculation shows the ECSA values of Pt@Pd-Fe/C, M-Pt@Pd-Fe/C and JM Pt/C are listed in table 2, respectively. The M-Pt@Pd-Fe/C catalyst has larger ECSA than Pt@Pd-Fe/C catalyst, which indicated that the M-Pt@Pd-Fe/C catalyst shows higher utilization of noble metal than Pt@Pd-Fe/C. The hydrogen absorption area of M-Pt@Pd-Fe/C is larger than that of Pt@Pd-Fe/C, which indicated the catalytic sites were

more exposed after acid treatment. In the oxidation region near to 0.75V vs. RHE in Fig.5 (b), the M-Pt@Pd-Fe/C catalyst shows a slight move towards higher potential, demonstrating that the binding strength of the adsorbed intermediates of M-Pt@Pd-Fe/C catalyst was weaker than that of JM Pt/C and Pt@Pd-Fe/C.

The curves of linear sweep voltammetry (LSV) test from the M-Pt@Pd-Fe/C catalyst in O_2-saturated $HClO_4$ electrolyte (0.1 M) for the ORR were supplied in Fig.5 (c), and the results of JM Pt/C, M-Pd-Fe/C, and Pt@Pd-Fe/C catalysts are also supplied as comparison. The catalytic activities can be shown by the half-wave potential ($E_{1/2}$). The M-Pt@Pd-Fe/C catalysts have the highest $E_{1/2}$ of 896 mv, about 15 mv and 7 mv higher than that of the JM Pt/C and Pt@Pd-Fe/C, respectively. This is the indication that the structure of the M-Pt@Pd-Fe/C catalyst has been changed and positively shifted metal oxide reduction profile could improve the catalytic activity. To further investigate the internal structure-function relationship and evaluate the mass-specific activities, the j_k was calculated by the following equation:[41]

$$j_k=(j_{lim}*j)/(j_{lim}-j) \quad (2)$$

Where j_{lim} is the diffusion-limited current at E=0.4 V, j is the current measured density at E =0.9V, and j_k is the kinetic current (A). The mass activities are also listed in table 2 according to the above equation.

In order to further study the performances of the obtained catalysts, the durability of the M-Pt@Pd-Fe/C catalyst was measured; Pt@Pd-Fe/C and JM Pt/C were tested for comparison. The durability tests were employed by repeating 10000 cycles between 0.06 and 1.10V as CV test and the scan speed was 500mV/s.[42] Fig.6 displays the $3000^{th,}$ 5000^{th} and 10000^{th} CV curves of of Pt@Pd-Fe/C, M-Pt@Pd-Fe/C, and JM Pt/C catalysts at durability potential cycles. After durability tests, we can see from Fig.6 (a) that JM Pt/C catalysts show the hydrogen absorption peak area decreases with potential cycles increase, demonstrating obviously poor durability. In Fig.6 (c) and (e), the M-Pt@Pd-Fe/C and Pt@Pd-Fe/C catalysts show minor changes in hydrogen adsorption peak area, indicating that the active sites were finely reserved. Compared with Pt@Pd-Fe/C and commercial JM Pt/C, the M-Pt@Pd-Fe/C catalysts show more promising durability, because of their obvious stable features on the hydrogen adsorption peaks. Fig.6 (b), (d) and (f) show initial and after durability test LSV

scans of Pt@Pd-Fe/C, M-Pt@Pd-Fe/C, and JM Pt/C catalysts. The M-Pt@Pd-Fe/C has the minimum decrease in $E_{1/2}$ when compare to this to Pt@Pd-Fe/C and JM Pt/C catalysts, this implies superior catalytic durability in oxidative environment. The negative shift in $E_{1/2}$ of the JM Pt/C, Pt@Pd-Fe/C, and M-Pt@Pd-Fe/C were calculated to be 41, 21, and 8 mV, respectively. The good stability of M-Pt@Pd-Fe/C could result from the modification of Pt atoms and remove of Fe element from the surface of inner core.

To study the catalytic mechanism of the M-Pt@Pd-Fe/C catalyst, LSV test with increasing rotation speed of the working electrode from 400 to 2500 rpm is conducted in O_2-saturated $HClO_4$ electrolyte, all LSV curves with Koutecky–Levich plots are shown in Fig.7.[43] The electron transfer numbers for the M-Pt@Pd-Fe/C catalyst were calculated to be 3.95 between 0.30 and 0.70 V, indicating a four-electron reaction mechanism occurs in the reduction process of O_2. This has further proved that M-Pt@Pd-Fe/C catalyst has superior ORR catalytic activity. The superior ORR activity and the catalytic mechanism of the M-Pt@Pd-Fe/C catalyst was further confirmed by rotating ring-disk electrode (RRDE) measurements.[44-45] The results are provided in Figure S2 which show good agreement with RDE analysis.

4. Conclusion

In summary, M-Pt@Pd-Fe/C catalyst synthesized using modified two-step reduction process and decorated with ultralow amount of Pt has effectively improved ORR catalytic performances over unmodified Pt@Pd-Fe/C catalysts. Thanks to the acid treatment partially substitute Fe atoms effectively modified the microstructure, the activity site of the modified Pd-Fe/C core for Pt decoration has increased, and the stability has been improved, these are vital characteristics for high performance ORR catalysts. After decoration with Pt, the catalyst demonstrated enhanced activity, such improvement can attribute to the strain effect and ligand effect between Pt, Fe and Pd. The work also demonstrated the Fe atoms on the surface of Pd-Fe/C core could reduce the stability, and partially removing them can effectively improve catalytic performances. The cost of our catalyst is also dramatically reduced compared to JM Pt/C. In a word, the strategy offered in this work can be feasible method for improving the catalytic activity and durability.

Acknowledgement

The authors would like to thank the financial supports from National Natural Science Foundation of China (No. U1705253, No. 51961145107, No. 21776014 and No. 21776012), the UK Engineering and Physical Sciences Research Council (EP/S032886/1), the National Key Research and Development Program of China (No. 2016YFB0101203), the International S&T Cooperation Program of China (No. 2013DFA51860) and the Fundamental Research Funds for the Central Universities (No. 12060093063).

References

[1] Arshad A, Ali HM, Habib A, Bashir MA, Jabbal M, Yan Y. Energy and exergy analysis of fuel cells: A review. Therm. Sci. Eng. Prog. 2019;9:308–321.

[2] Liu X, Xi J, Xu B-B, Fang B, Wang Y, Bayati M, Gao C. A High-Performance Direct Methanol Fuel Cell Technology Enabled by Mediating High-Concentration Methanol through a Graphene Aerogel. Small Methods. 2018;2:1800138.

[3] Kim C, Dionigi F, Beermann V, Wang X, Möller T, Strasser P. Alloy nanocatalysts for the electrochemical oxygen reduction (ORR) and the direct electrochemical carbon dioxide reduction reaction (CO_2RR). Adv. Mater. 2019;31:1–19.

[4] Wang X, Li Z, Qu Y, Yuan T, Wang W, Wu Y, Li Y. Review of metal catalysts for oxygen reduction reaction: from nanoscale engineering to atomic design. Chem. 2019;5:1486–1511.

[5] Luo M, Yang Y, Guo S. Precious metal nanocrystals for renewable energy electrocatalysis: structural design and controlled synthesis. Dalt. Trans. 2020;49:267–273.

[6] Shao M, Chang Q, Dodelet JP, Chenitz R. Recent advances in electrocatalysts for oxygen reduction reaction. Chem. Rev. 2016;116:3594–3657.

[7] Su L, Jia W, Li C-M, Lei Y. Mechanisms for Enhanced Performance of Platinum-Based Electrocatalysts in Proton Exchange Membrane Fuel Cells. ChemSusChem. 2014;7:361–378.

[8] Antolini E. The oxygen reduction on Pt-Ni and Pt-Ni-M catalysts for low-temperature acidic fuel cells: A review. Int J Energy Res. 2018;42:3747–3769.

[9] Anwar MT, Yan X, Asghar MR, Husnain N, Shen S, Luo L, Zhang J. Recent advances in hybrid support material for Pt-based electrocatalysts of proton exchange membrane fuel cells. Int J Energy Res. 2019;43:2694–2721.

[10] Liu X, Wu X, Scott K. Study of niobium and tantalum doped titania-supported Pt electrocatalysts for methanol oxidation and oxygen reduction reactions. Appl. Catal. B Environ. 2015;162:593–601.

[11] Liu X, Eileen HY, Scott K. Preparation and evaluation of a highly stable palladium yttrium platinum core–shell–shell structure catalyst for oxygen reduction reactions. J. Phys. Chem. Lett. 2016;7:1127–1137.

[12] Zhao Q, Wang C, Wang H, Wang J, Tang Y, Mao Z, Sasaki K. H_2-induced thermal treatment significantly influences the development of a high performance low-platinum core-shell PtNi/C alloyed oxygen reduction catalyst. Int J Energy Res. 2020;44:4773–4783.

[13] Alvar EN, Zhou B, Eichhorn SH. Composite-supported Pt catalyst and electrosprayed cathode catalyst layer for polymer electrolyte membrane fuel cell. Int J Energy Res. 2017;41:1626–1641.

[14] Liu X, Wu X, Scott K. Study of niobium and tantalum doped titania-supported Pt electrocatalysts for methanol oxidation and oxygen reduction reactions. Catal. Sci. Technol. 2014;4:3891–3898.

[15] Sebastián D, Baglio V, Aricò AS, Serov A, Atanassov P. Performance analysis of a non-platinum group metal catalyst based on iron-aminoantipyrine for direct methanol fuel cells. Appl. Catal. B Environ. 2016;182:297–305.

[16] Mun Y, Kim MJ, Park SA, Lee E, Ye Y, Lee S, Sung YE. Soft-template synthesis of mesoporous non-precious metal catalyst with Fe-N_x/C active sites for oxygen reduction reaction in fuel cells. Appl. Catal. B Environ. 2018;222:191–199.

[17] Chandran P, Ramaprabhu S. Catalytic performance of non-platinum-based hybrid carbon hetero-structure for oxygen reduction and hydrogen oxidation reactions in proton exchange membrane fuel cell. Int. J. Hydrogen Energy. 2018;43:18477–18487.

[18] Osmieri L, Escudero-Cid R, Videla AHM, Ocón P, Specchia S. Application of a non-noble Fe-NC catalyst for oxygen reduction reaction in an alkaline direct ethanol

fuel cell. Renew. Energy, 2018;115:226–237.

[19] Ji X, Gao P, Zhang L, Wang X, Wang F, Zhu H, Yu J. High-Performance Ordered PdCuFe/C Intermetallic Catalyst for Electrochemical Oxygen Reduction in Proton Exchange Membrane Fuel Cells. ChemElectroChem. 2019;6:3065–3070.

[20] Liu S, Xiao W, Wang J, Zhu J, Wu Z, Xin H, Wang D. Ultralow content of Pt on Pd–Co–Cu/C ternary nanoparticles with excellent electrocatalytic activity and durability for the oxygen reduction reaction. Nano Energy. 2016;27:475–481.

[21] Xiao W, Cordeiro MA, Gao G, Zheng A, Wang J, Lei W, Wang D. Atomic rearrangement from disordered to ordered Pd-Fe nanocatalysts with trace amount of Pt decoration for efficient electrocatalysis. Nano Energy. 2018;50:70–78.

[22] Wang D, Xin H-L, Yu Y, Wang H, Rus E, Muller DA, Abruña HD. Pt-decorated PdCo@Pd/C core-shell nanoparticles with enhanced stability and electrocatalytic activity for the oxygen reduction reaction. J. Am. Chem. Soc. 2010;132:17664–17666.

[23] Liu S, Zhang Q, Li Y, Han M, Gu L, Nan C, Dai Z. Five-fold twinned Pd_2NiAg nanocrystals with increased surface Ni site availability to improve oxygen reduction activity. J. Am. Chem. Soc. 2015;137:2820–2823.

[24] Liu S, Mu X, Li W, Lv M, Chen B, Chen C, Mu S, Cation vacancy-modulated PtPdRuTe five-fold twinned nanomaterial for catalyzing hydrogen evolution reaction, Nano Energy. 2019;61:346-351.

[25] Bao M, Amiinu IS, Peng T, Li W, Liu S, Wang Z, Pu Z, He D, Xiong Y, Mu S, Surface evolution of PtCu alloy shell over Pd nanocrystals leads to superior hydrogen evolution and oxygen reduction reactions, ACS Energy Lett. 2018;3:940-945.

[26] Ying J, Hu Z, Yang X, Wei H, Xiao Y, Janiak C, Mu S, Tian G, Pan M, Tendeloo G, Su B, High viscosity to highly dispersed PtPd bimetallic nanocrystals for enhanced catalytic activity and stability[J].Chem Commun. 2016;52:8219-8222.

[27] Ying J, Yang X, Hu Z, Mu S, Janiak C, Geng W, Pan M, Ke X, Tendeloo G, Su B, One particle@ one cell: highly monodispersed PtPd bimetallic nanoparticles for enhanced oxygen reduction reaction[J]. Nano Energy. 2014;8:214-222.

[28] Liu X, Zhang K, Lu J, Luo K, Gong J, Puthiyapura VK, Scott K. Determining the

Effect of Plasma Pre‐Treatment on Antimony Tin Oxide to Support Pt@Pd and the Oxygen Reduction Reaction Activity. ChemCatChem. 2015;7:1543–1546.

[29] Xiao W, Cordeiro MAL, Gong M, Han L, Wang J, Bian C, Wang D. Optimizing the ORR activity of Pd based nanocatalysts by tuning their strain and particle size. J. Mater. Chem. A. 2017;5: 9867–9872.

[30] Zhu H, Luo M, Zhang S, Wei L, Wang F, Wang Z, Han, K. Combined method to prepare core–shell structured catalyst for proton exchange membrane fuel cells Int. J. Hydrogen Energy. 2013;38:3323–3329.

[31] Wu Y, Liao S, Liang Z, Yang L, Wang R. High-performance core–shell PdPt@Pt/C catalysts via decorating PdPt alloy cores with Pt. J. Power Sources. 2009;194:805–810.

[32] Wang W, Wang R, Ji S, Feng H, Wang H, Lei Z. Pt overgrowth on carbon supported PdFe seeds in the preparation of core–shell electrocatalysts for the oxygen reduction reaction. J. Power Sources. 2010;195:3498–3503.

[33] Trinh QT, Yang J, Lee JY, Saeys M. Computational and experimental study of the Volcano behavior of the oxygen reduction activity of PdM@PdPt/C (M= Pt, Ni, Co, Fe, and Cr) core–shell electrocatalysts. J. Catal. 2012;291:26–35.

[34] Metin O, Mazumder V, Ozkar S, Sun S. Monodisperse nickel nanoparticles and their catalysis in hydrolytic dehydrogenation of ammonia borane. J. Am. Chem. Soc. 2010;132:7848–7849.

[35] Xiong Y, Yang Y, DiSalvo FJ, Abruña HD. Pt-decorated composition-tunable Pd–Fe@Pd/C core–shell nanoparticles with enhanced electrocatalytic activity toward the oxygen reduction reaction. J. Am. Chem. Soc. 2018;140:7248–7255.

[36] Mohanraju K, Kousik G, Cindrella L. Surfactant free synthesis of high surface area Pt@PdM_3 (M=Mn, Fe, Co, Ni, Cu) core/shell electrocatalysts with enhanced electrocatalytic activity and durability for PEM fuel cell applications. New J. Chem. 2016;40(10):8681-8695

[37] Zhu H, Li X, Wang F. Synthesis and characterization of Cu@Pt/C core-shell structured catalysts for proton exchange membrane fuel cell. Int. J. Hydrogen Energy. 2011,36: 9151–9154.

[38] Zhu H, Cai Y, Wang F, Gao P, Cao J. Scalable preparation of the chemically ordered Pt–Fe–Au nanocatalysts with high catalytic reactivity and stability for oxygen reduction reactions. ACS Appl. Mater. Interfaces. 2018;10:22156–22166.

[39] Alayoglu S, Zavalij P, Eichhorn B, Wang Q, Frenkel AI, Chupas P. Structural and architectural evaluation of bimetallic nanoparticles: a case study of Pt−Ru Core−Shell and alloy nanoparticles. ACS Nano. 2009;3:3127-3137

[40] He C, Liang Y, Fu R, Wu D, Song S, Cai R. Nanopores array of ordered mesoporous carbons determine Pt's activity towards alcohol electrooxidation. J. Mater. Chem. 2011;21:16357–16364.

[41] Liu Y, Chen N, Wang F, Cai Y, Zhu H. Pt–Co deposited on polyaniline-modified carbon for the electro-reduction of oxygen: the interaction between Pt–Co nanoparticles and polyaniline. New J. Chem. 2017;41: 6585–6592.

[42] Zhang L, Ji X, Wang X, Fu Y, Zhu H, Liu T-X. Chemically Ordered Pt–Co–Cu/C as Excellent Electrochemical Catalyst for Oxygen Reduction Reaction. J. Electrochem. Soc. 2020;167(2): 024507.

[43] Chen L, Guo H, Fujita T, Hirata A, Zhang W, Inoue A, Chen M. Nanoporous PdNi bimetallic catalyst with enhanced electrocatalytic performances for electro-oxidation and oxygen reduction reactions. Adv. Funct. Mater. 2011;21:4364–4370.

[44] Kong L, Liu X, Wei J, Wang S, Xu B, Long D, Chen F. T-Nb2O5 nanoparticle enabled pseudocapacitance with a fast Li-ion intercalation. Nanoscale. 2018;10:14165-14170.

[45] Tiwari J, Lee W, Sultan S, Yousuf M, Harzandi A, Vij V, Kim K. High-affinity-assisted nanoscale alloys as remarkable bifunctional catalyst for alcohol oxidation and oxygen reduction reactions. ACS Nano. 2017;11:7729-7735.

Scheme

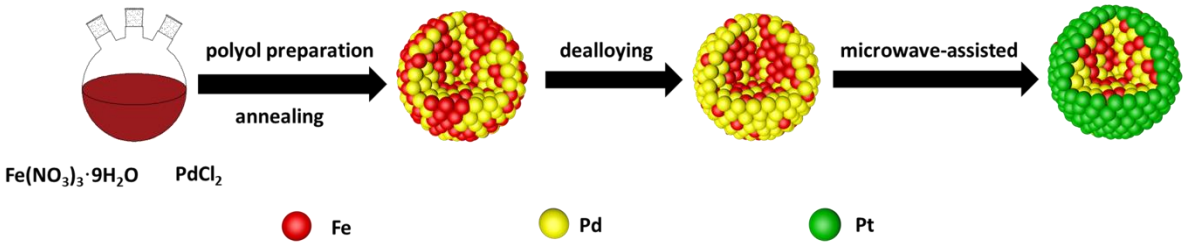

Scheme 1 the synthesis procedure of M-Pt@Pd-Fe/C

Figure

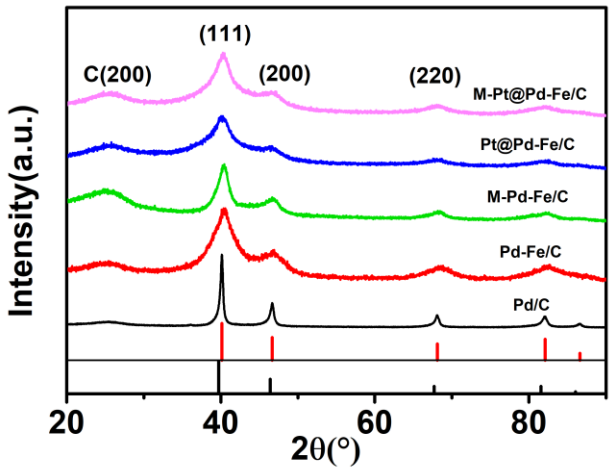

Fig.1 X-ray diffraction patterns of Pd/C, Pd-Fe/C, M-Pd-Fe/C, Pt@Pd-Fe/C, and M-Pt@Pd-Fe/C catalysts. The black and red vertical lines correspond to the peaks of intermetallic pure Pt (PDFcard # 04-0802) and pure Pd (PDFcard# 46-1043), respectively.

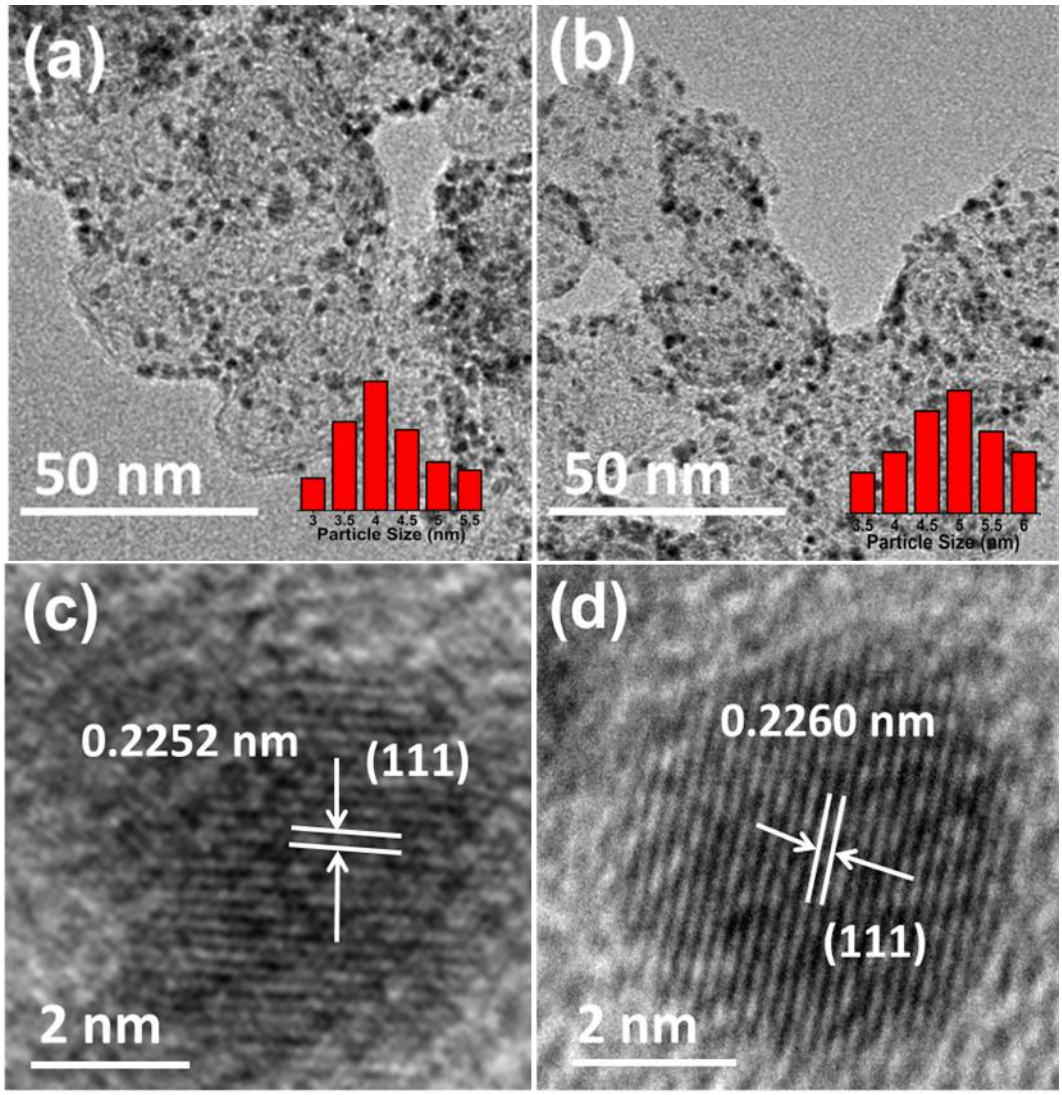

Fig. 2 TEM images and particle size distribution histograms of M-Pd-Fe/C (a) and M-Pt@Pd-Fe/C (b) catalysts; HRTEM images of M-Pd-Fe/C (c) and M-Pt@Pd-Fe/C (d) catalysts

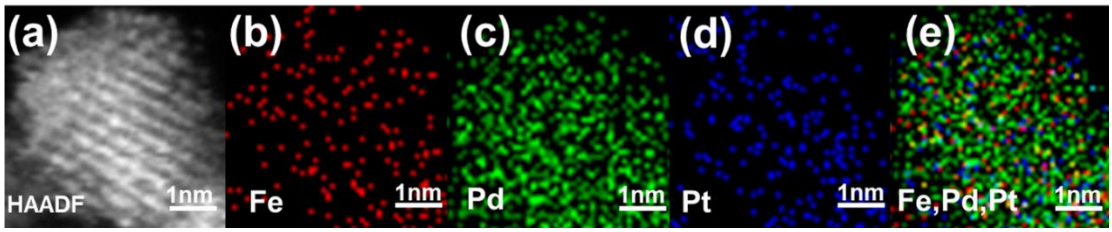

Fig.3 high magnification HAADF/STEM images of M-Pt@Pd-Fe/C (a) and EDS elemental mapping of Fe (b), Pd (c), Pt (d) and the composite (e).

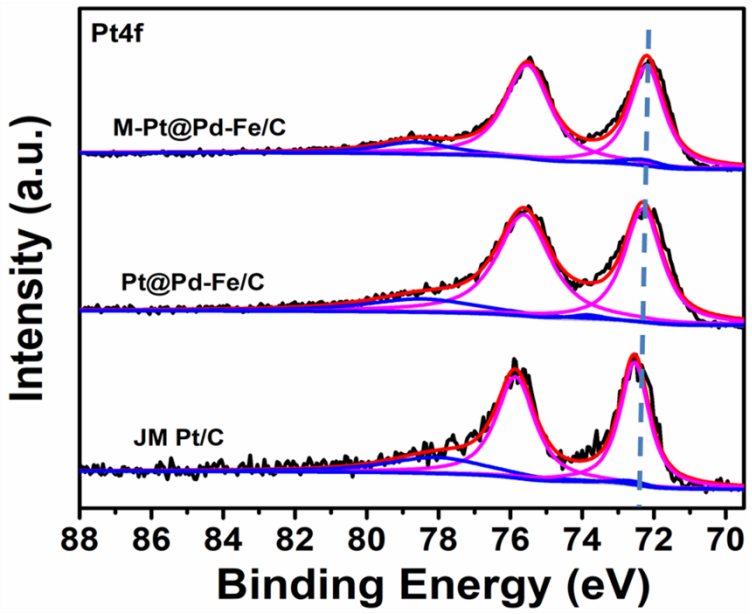

Fig.4 XPS spectra of JM Pt/C, Pt@Pd-Fe/C, and M-Pt@Pd-Fe/C catalysts in the Pt 4f region

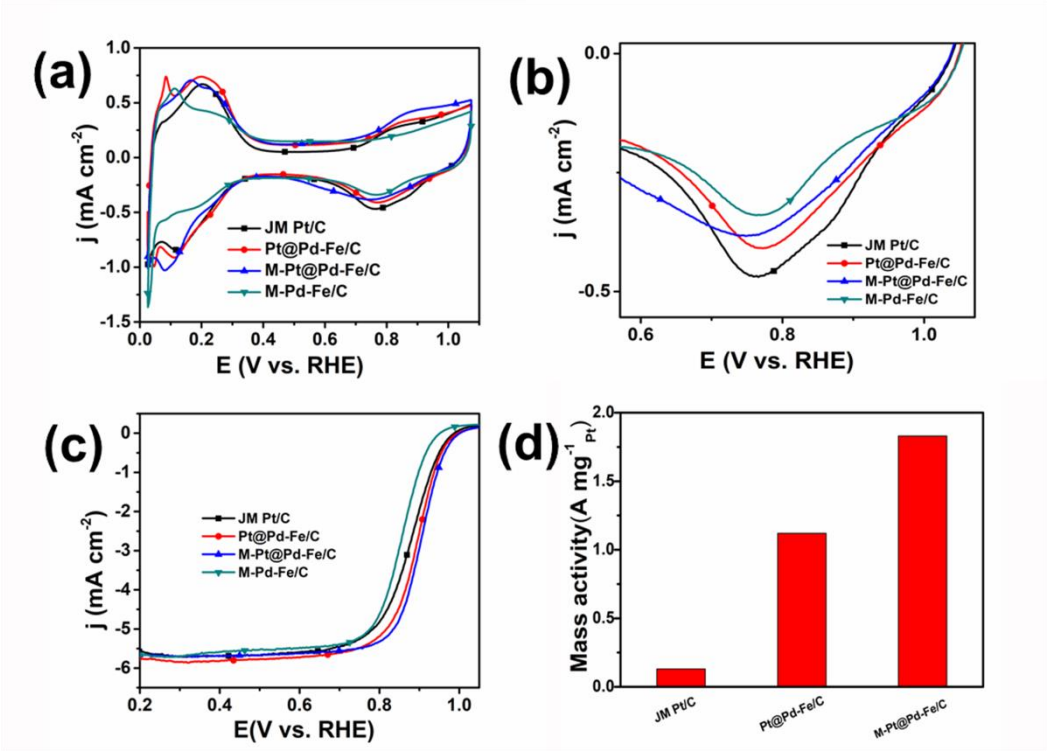

Fig. 5 Electrochemical testing results of JM Pt/C, M-Pd-Fe/C, Pt@Pd-Fe/C, and M-Pt@Pd-Fe/C catalysts, (a) CV curves, (b) expanded between 0.5 and 1.0 V vs. RHE, (c) ORR LSV curves and (d) Mass activities results of three selected catalysts

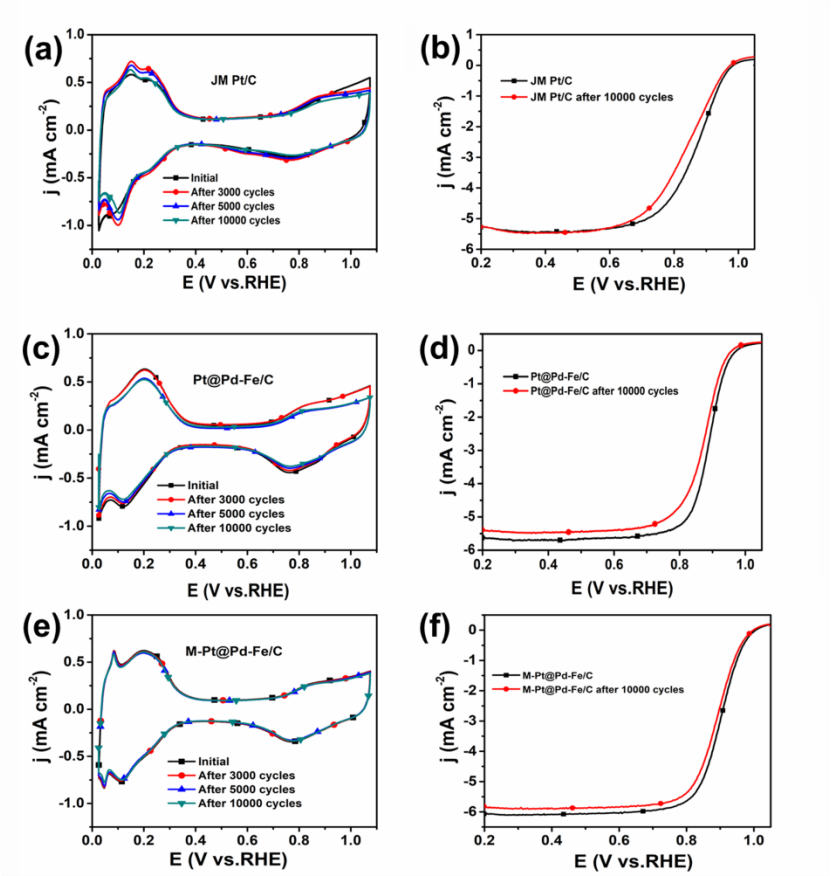

Fig. 6 CV durability test results for (a) JM Pt/C, (c) Pt@Pd-Fe/C and (e) M-Pt@Pd-Fe/C catalysts; and corresponding LSV durability test curves of (b) JM Pt/C (d) Pt@Pd-Fe/C and (f) M-Pt@Pd-Fe/C catalysts

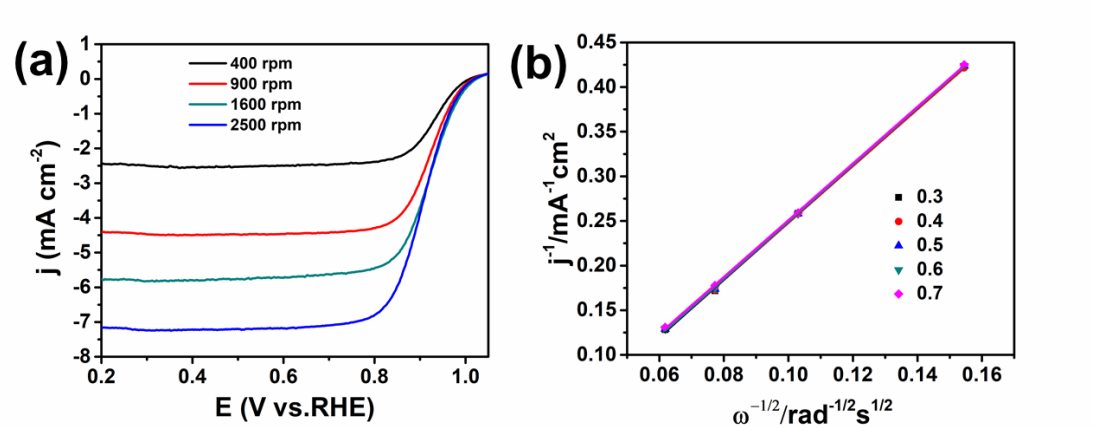

Fig.7 (a) LSV curves of M-Pt@Pd-Fe/C in O_2-saturated 0.1 M $HClO_4$ solution with different rotation rates and a scan rate of 10 mV s^{-1}; (b) Koutecky–Levich plots with linear fitting of M-Pt@Pd-Fe/C catalysts.

Tables

Table 1 Experimental composition of Pt@Pd-Fe/C and M-Pt@Pd-Fe/C.

Catalysts	**atomic ratio (ICP)**	**atomic ratio (EDX)**
Pt@Pd-Fe/C	$Pd_1Fe_{0.89}Pt_{0.03}$	$Pd_1Fe_{0.85}Pt_{0.03}$
M-Pt@Pd-Fe/C	$Pd_1Fe_{0.72}Pt_{0.03}$	$Pd_1Fe_{0.69}Pt_{0.03}$

Table 2 Electrochemical performance test results of different catalysts

Catalysts	**ECSA($m^2g^{-1}_{noble\ metal}$)**	**Mass activity($mA\ mg^{-1}_{Pt}$)**
JM Pt/C	72.56	0.13
Pt@Pd-Fe/C	64.90	1.12
M-Pt@Pd-Fe/C	68.07	1.83